Resources, Conservation & Recycling 222 (2025) 108495

Contents lists available at ScienceDirect

Resources, Conservation & Recycling

journal homepage: www.sciencedirect.com/journal/resources-conservation-and-recycling

Innovative sulfation strategy for efficient recovery of rare earth elements from spent fluorescent lamp powder

Hossein Shalchian *, Pietro Romano, Soroush Rahmati, Ionela Birloaga, Valentina Innocenzi, Francesco Vegliò

Department of Industrial and Information Engineering and Economics (DIIIE), Engineering Headquarters of Roio, University of L'Aquila 67100, L'Aquila, Italy

ARTICLE INFO

Keywords:
Spent fluorescent lamp
Rare earth elements
Sulfation
Hydrometallurgy
Flower-like REE mixed oxides

ABSTRACT

The recovery of rare earth elements (REEs) from spent fluorescent lamp phosphors is essential for resource sustainability and circular hydrometallurgy. While yttrium (Y) and europium (Eu) can be recovered through simple acid leaching, extracting cerium (Ce), lanthanum (La), and terbium (Tb) from green phosphors is challenging due to their resistance to dissolution. This study presents a novel sulfation-based process at relatively low temperatures to selectively recover REEs, particularly Tb, while minimizing energy consumption and environmental impact by preventing sulfuric acid and mercury evaporation.

Initially, sulfuric acid leaching selectively recovered most of Y and Eu, leaving other REEs in the solid residue. These elements were then precipitated as a nearly pure REE oxalate mixture (>99 % purity). The effects of sulfation time, temperature, and acid-to-powder weight ratio were optimized using Response Surface Methodology (RSM). Sulfation at 150 °C for 5 h enabled the recovery of nearly 100 % Ce and Gd, 98.01 % La, and 98.15 % Tb through water leaching. The mixed oxalate precipitate, enriched in La, Ce, and Tb, exhibited >98 % purity. SEM analysis revealed the formation of flower-like mixed REE oxides after calcination.

This process achieved high recovery efficiencies of 99.98 % Y, 100 % Eu, 99.92 % Ce, 97.22 % La, 97.68 % Tb, and 99.97 % Gd. By using only sulfuric and oxalic acid, it aligns with sustainable hydrometallurgy, reducing chemical diversity and enabling acid regeneration. This study provides an efficient, environmentally friendly approach for REE recovery from phosphor waste.

1. Introduction

Fluorescent lamps (FLs) have grown exponentially since the early 2000s, becoming a significant lighting source due to their energy efficiency, replacing the obsolete incandescent lamps (IL) technology. IL are known for their higher energy consumption, generating significant heat, and shorter lifetime, which have motivated their replacement. Today, light-emitting diodes (LED) replace FLs regarding energy efficiency; however, FLs are still widely used, especially in developing countries. FLs are responsible for large amounts of waste. According to recent estimates, fluorescent lamps accounted for approximately 33 % of global lighting sales in 2020, with many units still in use and destined for disposal in the coming years (Viana et al., 2022). The production and sale of FLs has been very high globally. In 2007, about 397 million compact FL units were sold in the U.S. and about 288 million units in Europe (Silveira and Chang, 2011; Tunsu et al., 2014). China produced 7 billion units in 2011 (Peng et al., 2014; Tan and Li, 2014). Despite a significant decline over the past decade due to LED adoption, particularly in Europe and the United States, in countries like India and China, FL still represents a substantial share of the lighting market. According to Market Research Future, the fluorescent lighting industry is expected to grow from USD 7.995 billion in 2024 to USD 16.506 billion by 2032, reflecting a compound annual growth rate (CAGR) of 9.48 % over the forecast period (2024–2032) (Dhapte, 2025). This continued production and use pose a serious environmental concern due to the improper disposal of spent lamps. Most FLs finish in municipal waste or open dumps, even in developed countries, contributing to pollution. For instance, in Europe, more than half of FLs are discarded improperly; in Brazil, only 11 % of the 2021 recycling target was met by 2019. Similarly, low recycling rates are reported in China, the Philippines, Sri Lanka, and even in countries like the U.S., Canada, and Japan, where rates remain between 7 % and 23 % (Viana et al., 2022).

* Corresponding author.
E-mail address: hossein.shalchian@univaq.it (H. Shalchian).

https://doi.org/10.1016/j.resconrec.2025.108495
Received 14 April 2025; Received in revised form 20 June 2025; Accepted 3 July 2025
Available online 5 July 2025

The inappropriate disposal of FL is a serious environmental problem. These lamps contain mercury (Hg), known for its high toxicity, and potentially hazardous metals. Another critical aspect is the presence of rare earth elements (REEs), essential elements for many modern technologies, including displays, batteries, wind turbines, and electric vehicles. Fluorescent lamps contain significant amounts of REEs, especially yttrium (Y), europium (Eu), cerium (Ce), lanthanum (La), and terbium (Tb). The phosphor used for luminescence behavior constitutes up to 2 wt % of FL and consists of a 9 to 26 % REEs content, significantly higher than REEs ore deposits (Dhawan and Tanvar, 2022).

The limited and concentrated mining of these resources in China (which holds about 90 % of the world's production) and the export restrictions imposed by this country in recent decades have forced many nations to find alternative sources of REEs, including the recycling of end-of-life electronic products and spent fluorescent lamps (Tan et al., 2015).

In the past decades, most studies have focused on the recovery of Y and Eu from red phosphors due to their relatively easy extraction and high economic value in spent fluorescent lamp powders (De Michelis et al., 2011; Innocenzi et al., 2017). However, recent research has shifted toward the comprehensive recovery of all REEs from this type of waste, with particular interest in Tb due to its exceptionally high value. Among REEs, Tb is the most expensive, with a significantly higher market price compared to others. However, its recovery presents a major challenge because it is primarily found in green phosphors, which are more chemically resistant and difficult to dissolve.

Several approaches have been explored to recover Tb, including high-temperature processes such as alkali fusion or acid fusion using molten salts at temperatures up to 950 °C, followed by acid leaching (Innocenzi et al., 2016; Ippolito et al., 2017; Porob et al., 2012; Tian et al., 2025; Vaz et al., 2025; Wu and al., 2014). In some cases, even more complex techniques, such as microwave-assisted alkali fusion combined with carbothermal reduction at elevated temperatures, have been employed before acid leaching (Liu et al., 2025). Other energy-intensive methods, including mechanical activation, have also been investigated (Ippolito et al., 2021; Song et al., 2017; Tan et al., 2017; Van Loy et al., 2017).

Despite these efforts, Tb recovery is often incomplete, even with these aggressive processes (Shukla and Dhawan, 2022). Furthermore, the use of high reagent concentrations and extreme temperatures, sometimes as high as 950 °C, adds to the complexity and cost of REEs extraction. These conventional methods are not ideal due to their reliance on highly corrosive chemicals, strict emission control requirements, and significant energy consumption. As a result, there is a growing need for more efficient, cost-effective, and environmentally friendly alternatives for the recovery of Tb and other REEs from spent fluorescent lamp powders.

Sulfation roasting and acid baking processes have also been employed to recover REEs from the phosphor powder of spent fluorescent lamps. Sulfation roasting involves an initial low-temperature baking of the powder with a sulfate source, followed by high-temperature roasting at 600–700 °C. In contrast, the acid baking process requires thermal treatment of the mixture at 200–300 °C, sometimes assisted by microwaves (Önal and Binnemans, 2019; Shukla and Dhawan, 2022; Shukla et al., 2021). While both methods achieve high REEs recovery rates, their major drawback is high energy consumption due to the elevated temperatures required. Additionally, sulfuric acid evaporation and decomposition to SO_3 poses a significant environmental concern in both sulfation roasting and acid baking, creating challenges for practical applications. This issue has not been adequately addressed in previous studies, despite the fact that many have employed temperatures as high as 200–500 °C, well beyond the boiling point of H_2SO_4 (337 °C) (Shukla and Dhawan, 2022; Shukla et al., 2021).

Therefore, developing a sulfation process that can safely and effectively treat spent fluorescent lamp powders at lower temperatures is both necessary and highly desirable. This study aims to design such a novel process, optimizing REEs recovery, particularly for Tb, while minimizing process temperature to overcome the limitations of conventional methods.

Furthermore, most previous studies have primarily focused on REEs leaching, overlooking the behavior of impurities during the process. In contrast, this study not only investigates REE recovery but also examines the dissolution and removal of impurities, providing a more comprehensive understanding of the system.

Another critical aspect often overlooked in REEs recovery from spent fluorescent lamps is the excessive use of diverse chemicals throughout the process. Many conventional methods, such as alkali fusion followed by acid leaching, involve multiple chemical reagents, increasing both complexity and environmental impact. In pursuit of a more sustainable hydrometallurgical approach, what can be termed circular hydrometallurgy, it is crucial to reduce chemical diversity and regenerate reagents wherever possible (Binnemans and Jones, 2023). This study embraces this philosophy by using only sulfuric acid for almost complete REE recovery, including Tb, and oxalic acid for precipitation. Additionally, sulfuric acid is regenerated within the process, ensuring a more sustainable and efficient recovery system.

2. Materials and methods

2.1. Materials

Spent fluorescent powder was obtained from the Relight Srl dismantling plant. A quantitative analysis of the phosphor powder was conducted through chemical digestion using aqua regia (HCl to HNO_3 in a 3:1 ratio) at 90 °C. Metal concentrations in the resulting solutions were determined using ICP-OES (Agilent Technologies 5100). The particle size distribution of the powder was measured using a particle size analyzer (Mastersizer 2000, Malvern Instruments Ltd.). Analytical-grade sulfuric acid (VWR Chemicals, >95 %) and oxalic acid (Fluka Chemika, >97 %) were used for the leaching, sulfation, and precipitation experiments, respectively.

2.2. Leaching and precipitation (acid leaching, water leaching)

The phosphors in spent fluorescent powder are typically a mixture of three main groups of red phosphor Y_2O_3: Eu^{3+} (YOX), green phosphor $LaPO_4$: Ce^{3+}, Tb^{3+} (LAP), GdB_5O_{12}: Ce^{3+}, Tb^{3+}, Mg^{3+} (CBT), $CeMgAl_{11}O_{19}$: Tb^{3+} (CMAT) and blue phosphor $BaMgAl_{10}O_{17}$:Eu^{2+} (BAM) (Binnemans et al., 2013; Innocenzi et al., 2018). Dissolving rare earth elements (REEs) from green and blue phosphors requires very aggressive conditions, whereas red phosphor can be dissolved using sulfuric acid (Van Loy et al., 2017). Therefore, the leaching experiments were divided into two stages. First, sulfuric acid leaching was performed to dissolve the red phosphor, selectively recovering yttrium and europium from the other REEs present in the green and blue phosphors. Eq. (1) shows the hypothesized sulfuric acid leaching reaction for Y and Eu from the red phosphor (Sadri et al., 2017):

$$REE_2O_3 + 6H^+ + 3(SO_4)^{2-} \rightarrow 2REE^{3+} + 3(SO_4)^{2-} + 3H_2O \quad (1)$$

where REE represents Y and Eu.

After recovering yttrium and europium via acid leaching, the solid residue, primarily composed of green phosphor, was treated through sulfation process. The sulfated samples were then subjected to water leaching to dissolve the remaining REEs. Eq. (2) demonstrates the hypothesized water leaching reaction of REE sulfate salts (Kim and Osseo-Asare, 2012):

$$REE_2(SO_4)_3 + nH_2O \rightarrow 2REE^{3+} + 3(SO_4)^{2-} + nH_2O \quad (2)$$

where REE represents Tb, Ce, La, Gd and any remaining Y and Eu.

All leaching experiments were conducted in a borosilicate glass

reactor at a preset temperature, with continuous stirring at 250 rpm. A vacuum filter with a 0.45 μm pore size was employed for solid-liquid phase separation, and all solutions were analyzed by ICP-OES (Agilent Technologies 5100) to determine leaching efficiency.

To recover REEs from the leaching solutions (from both the acid and water leaching steps), precipitation tests were performed by adding oxalic acid, as the most commonly used precipitant for REEs, to the leach liquors to precipitate REE oxalates as shown in Eq. (3) (Han, 2020):

$$2REE^{3+} + 3C_2H_2O_4 \rightarrow REE_2(C_2O_4)_3 + 6H^+ \quad (3)$$

where REE represents Y, Eu, Tb, Ce, La, and Gd. As observed, the oxalate precipitation reaction facilitates the regeneration of sulfuric acid in the process (Eq. (3)). These experiments were performed at room temperature for 1 hour. Afterward, the solid particles were filtered, and precipitation efficiency was determined by analyzing the final solutions using ICP. The precipitated REE oxalates were then calcined to obtain REE oxides as the final products, which were subsequently characterized using ICP, SEM (Philips), and XRD (Philips Panalytical instrument).

2.3. Sulfation process

These experiments aimed to recover Tb, Ce, La, and the remaining Gd after sulfuric acid leaching of Y and Eu. A statistical analysis was performed to assess the effects of different parameters on the sulfation process using an experimental design approach. Specifically, response surface methodology (RSM) with a central composite design (CCD) was employed, and the results were evaluated using analysis of variance (ANOVA) (Montgomery, 2017). The acid-to-powder weight ratio, temperature, and baking time were considered as independent variables. Supplementary Table S1 presents the levels of these variables used in the study. The experimental design included 14 experiments for the 3 independent variables, plus 3 center point runs to evaluate experimental error variance. This approach allows for the generation of the best mathematical model to predict the extraction efficiency of each REE as a function of the three independent variables within the selected ranges in Supplementary Table S1. Typically, a first- or second-order polynomial is used to generate the model based on significant parameters, as shown in Eqs. (4) and 5, which often provide good approximations for small design spaces:

$$y = \beta_0 + \sum_{i=1}^{k} \beta_i X_i \quad (4)$$

$$y = \beta_0 + \sum_{i=1}^{k} \beta_i X_i + \sum_{i=1}^{k} \beta_{ii} X_i^2 \sum_{i=1}^{k-1} \sum_{j=2}^{k} \beta_{ij} X_i X_j \quad (5)$$

In sulfation experiments, various amounts of sulfuric acid were added to the powder and mixed to create a homogeneous paste. The mixture turned gray, and the temperature increased as the sulfation reactions commenced. The homogenized pastes were then baked at different temperatures for varying durations according to the experimental design (Supplementary Table S1). All experiments were conducted in a random order to minimize systematic errors. Finally, the sulfated samples were leached in water to dissolve the REE sulfates, allowing the determination of the extraction efficiency of the sulfation process.

3. Results and discussion

3.1. Characterization of the spent fluorescent powder

The chemical composition of the spent fluorescent powder is presented in Table 1. Calcium and manganese originate from the white (HALO) phosphor. Yttrium and europium are primarily derived from YOX, or red phosphor, while cerium, lanthanum, and terbium mainly come from the LAP compound in green phosphor. The presence of gadolinium and boron indicates CBT (green phosphor) in the mixed phosphor powder. Aluminum is likely from CAT (green phosphor) and BAM (blue phosphor), and barium also originates from BAM.

Table 1
Chemical composition of the spent fluorescent powder determined by ICP-OES.

Element	Wt.%
Y	15.82 ± 0.26
Eu	0.97 ± 0.02
Ce	0.91 ± 0.02
La	1.39 ± 0.02
Tb	0.46 ± 0.01
Gd	0.35 ± 0.01
Ca	13.41 ± 0.33
Ba	2.24 ± 0.24
Al	1.69 ± 0.1
Fe	0.71 ± 0.05
Mn	0.35 ± 0.01
B	0.30 ± 0.01

Supplementary Figure S1 shows the XRD pattern and particle size distribution of the initial powder. The X-ray analysis revealed the presence of HALO phosphor ($Ca_{10}P_6O_{26}$), red phosphor (Y_2O_3), and green phosphor compounds ($CePO_4$, $EuMgAl_{11}O_{19}$) were detected in X-ray investigation. However, blue phosphor was not detected, likely due to its low concentration in the powder or interference and overlap with other peaks. The particle size distribution data indicates that 50 % of the particles are below 6.55 μm, 90 % are below 28.66 μm, and the maximum particle size is approximately 138 μm.

3.2. Thermodynamic evaluations

Sulfuric acid evaporation poses an environmental concern in sulfation and acid baking processes, representing a significant challenge in developing practical applications. This issue has not been adequately considered or addressed in previous studies, which have used temperatures as high as 200–500 °C, despite the boiling point of H_2SO_4 being around 337 °C (Shukla and Dhawan, 2022; Shukla et al., 2021). Therefore, selecting an appropriate temperature range that reduces sulfuric acid evaporation to a negligible level while maintaining a high reaction rate is crucial. Additionally, phosphorous powders that have not undergone mercury removal before REE extraction are at risk of Hg evaporation during acid baking processes, given mercury's boiling point of around 357 °C. Hence, it is also important to operate at temperatures that minimize Hg evaporation during sulfation and acid baking processes, particularly for samples that have not undergone prior mercury removal.

Supplementary Figure S2 shows the vapor pressure of H_2SO_4 and Hg as a function of temperature, calculated using HSC Chemistry® 10. As illustrated, the evaporation rate becomes significant for both substances at temperatures above 200 °C. Since thermal treatment of the powder and acid mixture at temperatures above 200 °C is categorized as the acid baking process, and at lower temperatures as the sulfation process (Shukla et al., 2021), it is clear that sulfuric acid evaporation has been a significant issue in studies using acid baking at these higher temperatures, an issue that has not been adequately addressed. Conversely, Supplementary Figure S2 demonstrates that evaporation is negligible at temperatures below 150 °C, with vapor pressures between 0.003–0.004 atm at 150 °C for both substances, indicating a safe operating temperature for the sulfation process of spent fluorescent powder.

For spent fluorescent powders containing mercury, after sulfation within the above temperature range, it is expected that Hg will remain in the solid residue after water leaching. This is due to the positive standard Gibbs free energy values of the hypothesized sulfation reactions of Hg, as shown below (Eqs. (6) and 7):

$$2Hg + H_2SO_4 \rightarrow Hg_2SO_4 + H_2 \quad \left[\Delta G^0_{25^\circ C} = 64.21\ kJ\ \Delta G^0_{150^\circ C} = 62.16\ kJ\right] \tag{6}$$

$$Hg + H_2SO_4 \rightarrow HgSO_4 + H_2 \quad \left[\Delta G^0_{25^\circ C} = 141.06\ kJ\ \Delta G^0_{150^\circ C} = 124.27\ kJ\right] \tag{7}$$

Therefore, the final solid residue after water leaching can be treated separately for Hg removal in a safe manner.

The hypothesized sulfation reactions for the main oxides and phosphate compounds of REEs present in red and green phosphors are shown below (Eqs. (8)–14). The variations in the standard Gibbs free energy values of these reactions as a function of temperature were calculated using HSC Chemistry® 10, and the results are illustrated in Supplementary Figure S3. As noted earlier, the red phosphor primarily consists of yttrium and europium oxides, while the green phosphor contains phosphates of La, Ce, and Tb. For Gd, which is typically found in the GdB_5O_{12} compound (CBT) (Innocenzi et al., 2018), thermodynamic data were not available in the software's database. Therefore, sulfation reactions for gadolinium oxide and phosphate were considered instead.

$$Y_2O_3 + 3H_2SO_4 = Y_2(SO_4)_3 + 3H_2O \tag{8}$$

$$Eu_2O_3 + 3H_2SO_4 = Eu_2(SO_4)_3 + 3H_2O \tag{9}$$

$$Gd_2O_3 + 3H_2SO_4 = Gd_2(SO_4)_3 + 3H_2O \tag{10}$$

$$2LaPO_4 + 3H_2SO_4 = La_2(SO_4)_3 + 2H_3PO_4 \tag{11}$$

$$2CePO_4 + 3H_2SO_4 = Ce_2(SO_4)_3 + 2H_3PO_4 \tag{12}$$

$$2TbPO_4 + 3H_2SO_4 = Tb_2(SO_4)_3 + 2H_3PO_4 \tag{13}$$

$$2GdPO_4 + 3H_2SO_4 = Gd_2(SO_4)_3 + 2H_3PO_4 \tag{14}$$

Supplementary Figure S3 demonstrates negative standard Gibbs free energy values for sulfation reactions across the entire temperature range, except for $TbPO_4$, $GdPO_4$ (if present in the powder), and $CePO_4$ with negative values up to 119 °C, 149 °C, and 249 °C, respectively. According to these predictions, sulfation reactions for all investigated REEs are theoretically feasible up to 150 °C, except for Tb, which is feasible only up to 119 °C. Although the sulfation reaction is theoretically feasible at lower temperatures for all the mentioned compounds, in practical conditions using sulfuric acid solutions, as previously noted, only Y and Eu can be efficiently recovered from the red phosphor below the boiling point of water. Most of the Ce, La, and Tb remain as unreacted phosphates in the solid residue. Consequently, extracting these latter REEs from green phosphor requires more harsh conditions, such as higher temperatures and acid concentrations, making the sulfation process necessary instead of the acid leaching process.

3.3. Y and Eu recovery by acid leaching and precipitation

According to the above results and literature, dissolving REEs from green and blue phosphors requires very harsh conditions, whereas red phosphor can be dissolved with high efficiency using sulfuric acid (et al., 2017). Therefore, a sulfuric acid leaching step was performed to selectively dissolve the red phosphor, enabling the recovery of yttrium and europium from the other REEs present in the green and blue phosphor.

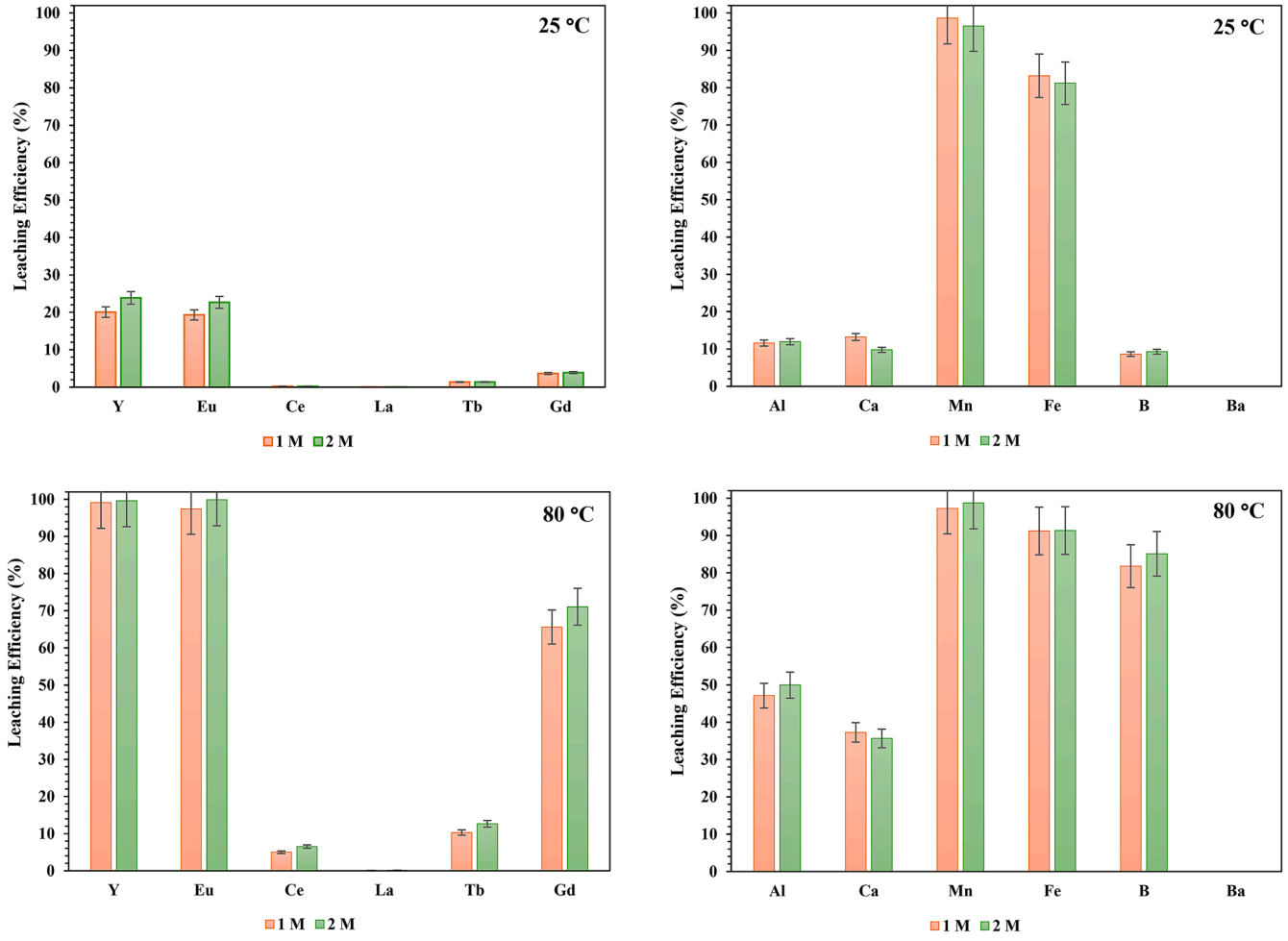

Fig. 1. Effect of sulfuric acid concentration and temperature on the leaching efficiency of REEs and impurities (1 hour of mixing at a solid-to-liquid ratio of 5 %).

Consequently, Y and Eu can be dissolved from red phosphors according to Eq. (1).

Leaching experiments were conducted at 25 °C and 80 °C using sulfuric acid concentrations of 1 M and 2 M, with a solid-to-liquid ratio of 5 %. The reaction time was 1 h, and the mixture was stirred constantly at 250 rpm. The results are shown in Fig. 1. It is evident that sulfuric acid concentration has no significant effect on the leaching efficiency of REEs and impurities. Fig. 1 demonstrates high selectivity in the leaching of Y and Eu over Ce, La, and Tb across both temperatures and acid concentrations. The effect of temperature, however, is significant for the leaching efficiency of Y and Eu which are present in red phosphor and Gd which is present in green phosphor. Gadolinium likely originates from GdB_5O_{12}:Ce^{3+}, Tb^{3+} (CBT), consistent with the partial dissolution of Ce and Tb, which increases with temperature, probably from this oxide. Cerium and terbium may also originate from $EuMgAl_{11}O_{19}$: Ce^{3+}, Tb^{3+} (as shown in Supplementary Figure S1). This indicates that CBT and CMAT dissolve more readily than phosphates containing La, Ce, and Tb. Furthermore, the results suggest that the majority of Ce and Tb, along with all La, exist in the phosphate form $CePO_4$:La^{3+}, Tb^{3+} (Supplementary Figure S1).

For the impurities, barium originating from the blue phosphor (BAM), forms insoluble barium sulfate during leaching and therefore remains in the solid residue (Fig. 1). The leaching efficiency of aluminum, derived from CMAT and BAM, increases with temperature, similarly to cerium and terbium. As expected, the dissolution rate of boron also rises with temperature, like gadolinium, due to their shared origin (CBT). Manganese, originating from HALO phosphor which is soluble in sulfuric acid. Consequently, the leaching efficiency of Mn is high even at room temperature.

In order to recover REEs from solution after leaching at 80 °C, some precipitation experiments were performed using oxalic acid. Rare earth elements can be recovered as oxalates (Ippolito et al., 2017) by adding oxalic acid to the leach liquor as represented in Eq. (3). Hence, precipitation behavior of REEs was evaluated by adding different values of oxalic acid. Fig. 2 Illustrates precipitation efficiency of REEs and impurities versus added values of oxalic acid as its concentration in the solution. As can be seen the precipitation efficiency of REEs increased by oxalic acid value significantly, up to 0.15 M oxalic acid. Adding more values of oxalic acid didn't affect the precipitation efficiency of REEs significantly. On the other hand, the precipitation efficiency of impurities is almost zero, except for calcium which is increased above 0.15 M of oxalic acid. Consequently, a 0.15 M oxalic acid is effective to precipitate the majority of REEs selectively from the leaching acid solution, resulting in almost pure REEs oxalates mixture with 99.17 % purity, which contains 93.44 % of yttrium oxalate hydrate, 4.05 % of europium oxalate hydrate, 1.12 % gadolinium oxalate hydrate, 0.28 % terbium oxalate hydrate, 0.27 % cerium oxalate hydrate, 0.01 % lanthanum oxalate hydrate, and 0.83 % calcium oxalate and calcium sulfate.

The precipitated REE oxalate mixture was analyzed using XRD, TGA-DTA, and SEM. Fig. 3 presents the characterization results of the final product, both before and after calcination. The XRD pattern of the precipitate reveals two forms of yttrium oxalate hydrate as the main phases in the final precipitate. TGA-DTA analysis was performed to determine the optimal temperature for calcination to convert REE oxalates into oxides. As shown in Fig. 3-c, yttrium oxalate hydrates lose water in two stages: the first below 200 °C and the second below 400 °C. Subsequently, the dehydrated oxalate begins to decompose into yttrium oxide, with the reaction completing at 700 °C. This temperature is higher than the value reported in the literature, likely due to differences in the composition of the mixed oxalate (Mesaros et al., 2015), but almost the same results obtained in a recent study (Bilen et al., 2025). Based on TGA results, the yttrium oxalate hydrate mixture was calcined at 700 °C for 1 h.

The XRD pattern of the calcined sample confirms yttrium oxide as the main product, with europium oxide sulfate identified as a byproduct of the calcination process (Fig. 3-b). Particle size distribution analysis indicates minimal change in size and distribution before and after calcination, implying that the calcination process had little effect on particle size (Fig. 3d-e).

SEM images of the sample reveal irregularly grown crystals of yttrium oxalate hydrate prior to calcination. After calcination, some particles developed a flower-like morphology (Fig. 3-i). Thus, SEM analysis demonstrates the formation of yttrium oxide with a flower-like morphology, recovered from spent fluorescent lamp powder.

3.4. Tb, La, Ce recovery by sulfation followed by water leaching and precipitation

The solid residue remaining after sulfuric acid leaching of yttrium and europium was subjected to a sulfation process to investigate the effects of key parameters on the recovery of terbium, lanthanum, and cerium. Response Surface Methodology (RSM) with a Central Composite Design (CCD) was employed, using the parameter levels indicated in Supplementary Table S1. The results were analyzed using Analysis of Variance (ANOVA).

Following the sulfation process, the solid residue was leached in water to dissolve and recover rare earth element sulphates (Eq. (2)). Preliminary water leaching experiments indicated that a 10 % solid-to-liquid (S/L) ratio and a leaching time of 10 min were sufficient to dissolve nearly all leachable REE sulphates from the solid obtained after

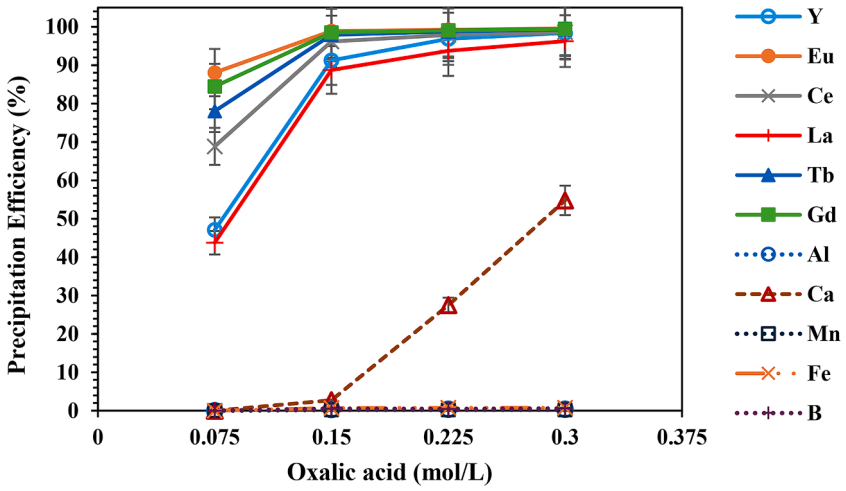

Fig. 2. Effect of oxalic acid value on the precipitation of REEs and impurities after sulfuric acid leaching (1 h of reaction time at room temperature).

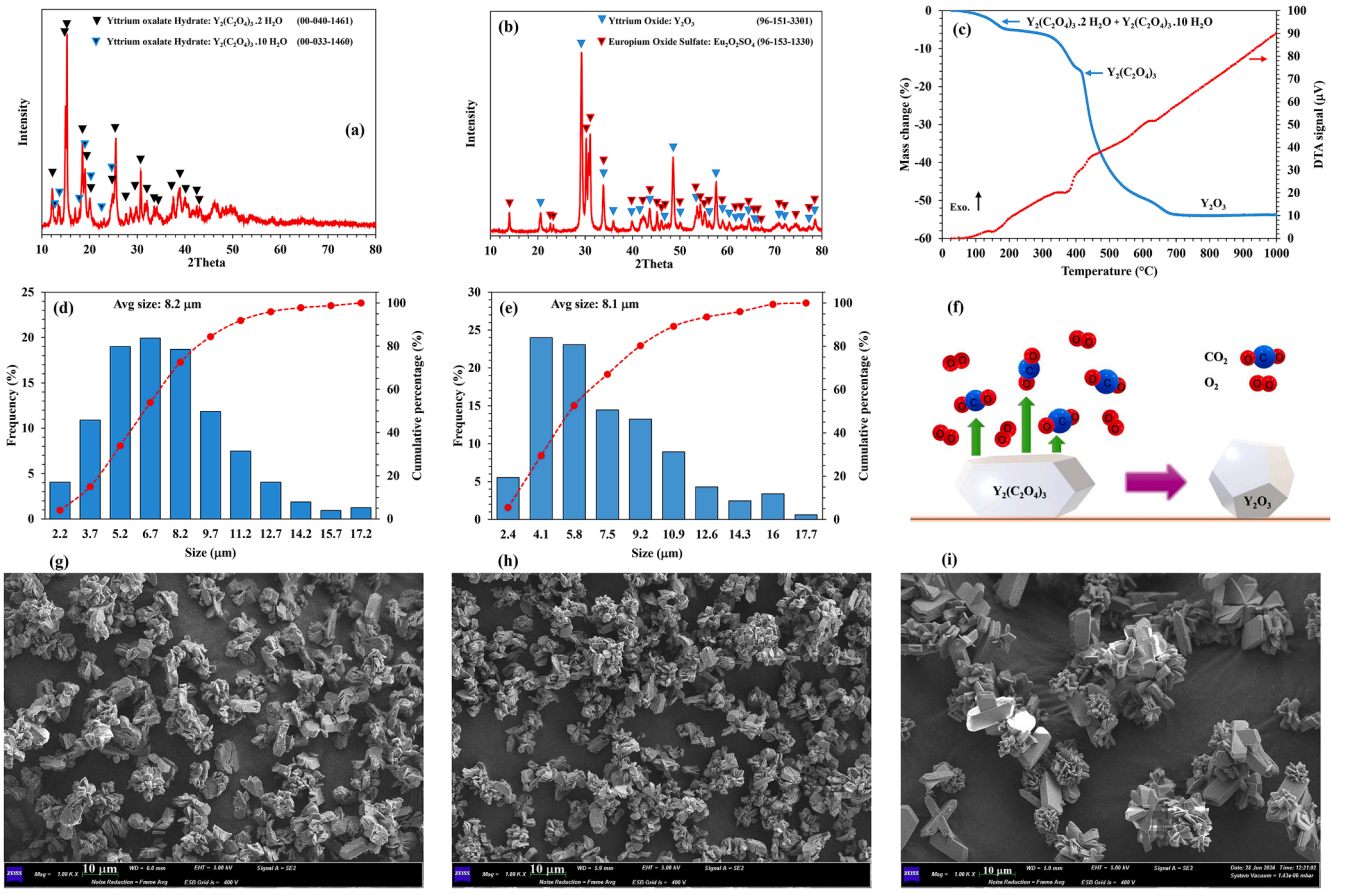

Fig. 3. (a) XRD pattern of the yttrium and europium oxalate, (b) XRD pattern of the yttrium and europium oxides after calcination, (c) TGA-DTA graph of the yttrium and europium oxalate in the presence of air with a heating rate of 10 °C/min, (d) and (e) particle size distribution of the yttrium and europium oxalate before and after calcination, (f) schematic view of the calcination process of yttrium oxalate in the presence of oxygen, (g) SEM image of yttrium and europium oxalate, (h-i) SEM image of yttrium and europium oxides after calcination.

sulfation (results not shown here). Consequently, all solids underwent leaching under these conditions at room temperature and 250 rpm.

Supplementary Table S2 presents REE recovery results after sulfation and water leaching. It is important to note that the recovery percentages of Y, Eu, Gd and the other REEs are based on the remaining amounts of these elements in the solid residue after the initial sulfuric acid leaching. As shown in the table, the results demonstrate an almost complete recovery of all REEs, particularly terbium at 150 °C, after 5 h with an acid-to-powder weight ratio of 2. This is significant because terbium is the most valuable REE in phosphor powder and one of the most challenging to recover, often exhibiting lower recovery efficiency in previous studies (Ippolito et al., 2021; Shukla and Dhawan, 2022). These findings highlight the effectiveness of the sulfation process in achieving complete REE recovery from spent fluorescent lamp powder.

Analysis of variance was performed to model the leaching efficiency of different REE according to the results in Supplementary Table S2. In ANOVA, the P-value criterion was used to determine significant parameters. A P-value of <0.05 indicates that the model terms are statistically significant. Accordingly, insignificant parameters were removed during the model development. Supplementary Table S3-S8 show the results of ANOVA for Y, Eu, Ce, La, Tb, and Gd. The obtained models for predicting recovery efficiencies are summarized in Supplementary Table S9.

Supplementary Figure S4 illustrates the model-fitted results versus the actual values for REE recovery, plotted based on the models presented in Supplementary Table S9. As shown in Supplementary Figure S4, the data for Y, Eu, and Gd are more scattered compared to Ce, La, and Tb, which can be attributed to their different origins. This observation aligns with the adjusted R^2 values presented in Supplementary Table S9. A better fit between the models and actual values is observed for Ce, La, and Tb, indicating more accurate model predictions for these three REEs.

Based on the fitted models and the coefficients of key parameters (Supplementary Table S9), it is evident that the recovery efficiency of Y and Eu depends primarily on the acid-to-powder weight ratio and the temperature during the sulfation process. Among these, the acid-to-powder weight ratio has a more significant effect than temperature. This similar behavior can be attributed to the shared origin of Y and Eu, both of which originate from red phosphor and were largely recovered during the initial sulfuric acid leaching.

Gadolinium exhibits a similar pattern but also shows dependency on the sulfation time.

Supplementary Figure S5 presents 3D response surface plots for REE recovery efficiencies, generated from the fitted models based on the three key parameters: sulfation time, temperature, and acid-to-powder weight ratio for Y, Eu, and Gd. The dependency of Y and Eu on temperature and acid-to-powder weight ratio, along with their independency to sulfation time, is clearly evident in the first two rows of Supplementary Figure S5, consistent with the data in Supplementary Table S9.

The curvature observed in the response surfaces is attributed to second-order terms such as A^2 and T^2. In contrast, the last row of Supplementary Figure S5 displays flat response surfaces for Gd, indicating that its recovery is influenced solely by the three main parameters without any significant interaction effects or second-order terms.

Therefore, for these elements, the recovery efficiency is mainly

influenced by the acid-to-powder weight ratio, with temperature being the least significant factor and sulfation time playing a role only in the case of Gd.

For Ce, La, and Tb, which primarily originate from green phosphor ($CePO_4$: La^{3+}, Tb^{3+}), all three key parameters, along with nearly all their interaction factors and the second-order terms were identified as significant model terms. The coefficients for these elements fall within a similar range, indicating that they undergo the same sulfation and dissolution mechanisms, as is revealed in Supplementary Figure S6 by the similar responses.

According to Supplementary Figure S6, the recovery rates of Ce, La, and Tb are highly dependent on sulfation temperature, followed by the acid-to-powder weight ratio, particularly at higher temperatures, and sulfation time. These three key parameters exhibit strong curvature in all graphs, highlighting the significance of interaction effects and second-order model terms for these REEs.

As previously discussed, the fitted models for Ce, La, and Tb demonstrate a strong ability to predict recovery efficiency within the studied parameter space, as indicated by their high adjusted R^2 values.

Supplementary Table S10 presents the results of impurity leaching following sulfation and water leaching. ANOVA was conducted to identify the significant parameters influencing the recovery and leaching of impurities during the sulfation-water leaching process, enabling the modeling of leaching rates based on the data in Supplementary Table S10. Supplementary Tables S11-S15 summarize the ANOVA results for Al, Ca, Mn, Fe, and B after eliminating insignificant model terms according to the 0.05 P-value criterion. The final models predicting the leaching rates of these impurities are presented in Supplementary Table S16.

Supplementary Figure S7 illustrates the model-fitted results versus the actual values for impurity leaching, plotted based on the models in Supplementary Table S16. As shown, data for Al and Ca exhibit greater scatter compared to Mn, Fe, and B, which aligns with the adjusted R^2 values in Supplementary Table S16. This variation can be attributed to differences in impurity origins, as well as the limited solubility of calcium sulfate, which resulted in leaching efficiency values being scattered within a narrow range of 13–18 % (Supplementary Table S10).

According to the fitted models and the coefficient values in Supplementary Table S16, aluminum and calcium dissolution are primarily influenced by sulfation time and temperature, while manganese dissolution depends on temperature and the acid-to-powder weight ratio. In contrast, boron recovery is governed by all three key parameters, whereas iron dissolution is influenced by these three parameters along with nearly all their interaction terms and second-order effects.

Supplementary Figures S8 and S9 present 3D response surface plots for impurity dissolution rates, generated from the fitted models based on the three key parameters (Supplementary Table S16). The curvature observed in the response surfaces, particularly for Ca, Mn, and Fe, is attributed to second-order terms such as A^2, t^2, and T^2. In contrast, the flat response surfaces for boron indicate that its recovery is determined only by the three main parameters, without significant second-order effects.

In conclusion, according to the above results, increasing the three key parameters not only enhances the recovery rate of REEs but also promotes the dissolution of impurities. However, given that the primary objective is to maximize REE recovery while minimizing impurity leaching, the priority remains achieving the highest possible REE recovery, even at the expense of increased impurity dissolution. Therefore, the next step will focus on selective recovery of REEs from the leaching solution to obtain a relatively pure mixture of REEs oxides.

To recover REEs from the leaching solution, an oxalate precipitation approach was employed (Eq. (3)). Preliminary precipitation experiments were conducted using varying concentrations of oxalic acid. Before the addition of oxalic acid, the solution pH was increased to 1 to facilitate oxalic acid dissolution (Chi and Xu, 1999) . These experiments revealed that a final oxalic acid concentration of 0.3 M was optimal, effectively precipitating 90.40 % Y, 99.20 % Eu, 97.14 % Ce, 92.28 % La, 98.63 % Tb, and 98.97 % Gd while minimizing impurity precipitation. These results show more efficient usage of oxalic acid than those reported in a previous study, which used 80 g/L oxalic acid (~0.88 M) to precipitate 95 % of REEs from a chloride solution system which contained only about 34.6 ± 1.52 mg/L of total REEs (Nawab et al., 2022).

Thus, a 0.3 mol oxalic acid per liter of the leaching solution proved to be effective in selectively precipitating the majority of REEs from the water leaching solution, yielding an almost pure REE oxalate mixture with 98.56 % purity. ICP results and mass balance calculations, supported by XRD evaluations, confirmed that the final oxalate precipitate is a decahydrate compound composed of approximately 43.72 % lanthanum oxalate hydrate, 27.35 % cerium oxalate hydrate, 14.86 % terbium oxalate hydrate, 7.31 % yttrium oxalate hydrate, 3.97 % gadolinium oxalate hydrate, 1.36 % europium oxalate hydrate, and 1.44 % calcium oxalate and calcium sulfate.

The precipitated REE oxalate mixture was analyzed using XRD, TGA-DTA, and SEM. Fig. 4 presents the characterization results of the final product, both before and after calcination. The XRD pattern of the precipitate (Fig. 4-a) identifies cerium oxalate decahydrate as the predominant phase, representing all other REE oxalates in the sample, with a general formula of $RE_2(C_2O_4)_3{\cdot}10H_2O$, where RE denotes Ce, La, Tb, Gd, Y, and Eu.

TGA-DTA analysis was conducted to determine the optimal calcination temperature for converting REE oxalates into oxides. As shown in Fig. 4-c, REE oxalate decahydrate undergoes dehydration up to 397 °C, losing ten water molecules with an endothermic peak primarily between 120 and 200 °C. The observed weight loss of 25.7 % closely aligns with the average theoretical value of 25.03 % for all mentioned REEs in the sample as $RE_2(C_2O_4)_3{\cdot}10H_2O$. Beyond this point, the dehydrated oxalate ($RE_2(C_2O_4)_3$) begins decomposing into mixed REE oxides, exhibiting a main exothermic peak around 400 °C. The decomposition process is completed at approximately 800 °C, after which no further weight loss is observed. These temperatures are higher than those reported in the literature for pure cerium oxalate, where the endothermic peak for water removal occurs at 130 °C and the exothermic peak for oxalate decomposition is observed at 320 °C (Altaş and Tel, 2001). This discrepancy is attributed to the presence of a mixed oxalate compound in the current study. The total weight loss of 52 % is consistent with the theoretical weight loss of 54 % for the RE oxalate decahydrate mixture, accounting for 2–3 % calcium compounds as the main impurities in the final oxide product. Based on these TGA results, the mixed RE oxalate decahydrate was calcined at 800 °C for one hour.

The XRD pattern of the calcined sample (Fig. 4-b) identifies gadolinium cerium oxide and terbium oxide as the primary products, along with calcium oxalate as a byproduct of the calcination process. Similar to the pre-calcination oxalate phase, gadolinium cerium oxide can be considered representative of all REE oxides in the sample, forming a mixed oxide phase. Particle size distribution analysis indicates a reduction in both average particle size and distribution range after calcination, suggesting that the process facilitated crystallization of oxide phases with smaller particle sizes (Fig. 4d-e).

SEM investigations further confirm the reduction in particle size before and after calcination, as illustrated in Fig. 4 g and Fig. 4-h, with Fig. 4-h captured at a higher magnification. Morphological analysis reveals a combination of flower-like and wafer-slab-like structures both before and after calcination. Somehow a similar morphology was also observed for cerium oxalate and lanthanum oxalate by other researchers (Alcaraz et al., 2022; Liascukiene et al., 2021). At higher magnifications, significant structural changes become apparent (Fig. 4-i and Fig. 4-f), where small spherical nanoparticles (<100 nm) and thin flakes (~400–500 nm) have crystallized on the surface of primary flakes along preferential orientations (Fig. 4-f).

Thus, SEM analysis confirms the formation of mixed oxide particles with wafer-slab-like and flower-like morphologies, decorated with nanometric particles and flakes, successfully recovered from spent

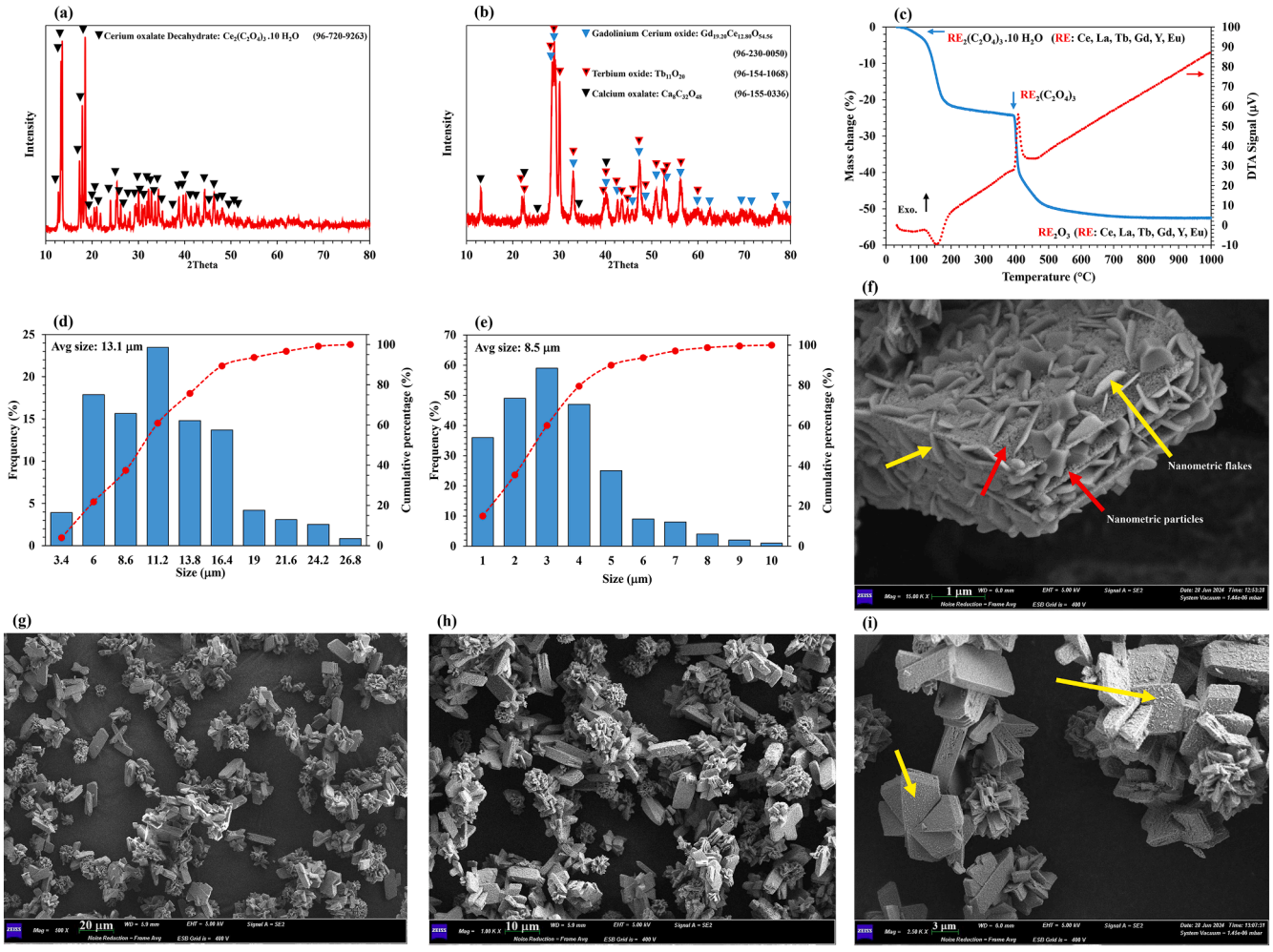

Fig. 4. (a) XRD pattern of the precipitated oxalate after the sulfation-water leaching process, (b) XRD pattern of the oxalate precipitate after calcination, (c) TGA-DTA curve of the precipitated oxalate in air at a heating rate of 10 °C/min, (d, e) particle size distribution of the precipitated oxalate before and after calcination, (f) high-magnification SEM image of an oxide particle after calcination, (g) SEM image of the precipitated oxalate, (h, i) SEM images of the obtained oxide after calcination at different magnifications, highlighting the various morphologies of the crystallized oxides.

fluorescent lamp powder.

Finally, both products obtained after oxalic acid precipitation, before and after calcination, were analyzed using SEM coupled with elemental analysis. Supplementary Figure S10-a presents an SEM image of the oxalate particles precipitated from the sulfuric acid leachate during the yttrium and europium recovery stage. The corresponding elemental spectrum identifies Y, Eu, Gd, C, and O as the primary elements, with Ca and S as impurities, aligning with previous ICP purification evaluations and previous results (Fig. 1–3). Elemental mapping further confirms the distribution of these elements within the selected particle, demonstrating a higher concentration of Y and Eu relative to Gd, which is consistent with prior findings.

As expected, the same elements were detected in the spectrum after calcination, with sharper peaks due to element enrichment following weight loss from thermal decomposition (Supplementary Figure S10-b). The elemental maps of the calcined sample indicate an overall increase in element concentrations, including Gd, compared to the pre-calcination sample.

Supplementary Figure S10-c illustrates the elemental spectrum and corresponding mapping of the oxalate precipitate obtained after the sulfation-water leaching process, which targeted REE recovery from the green phosphor. The spectrum confirms the presence of Ce, La, Tb, Y, Eu, Gd, C, O, Ca, and S, in agreement with previous analyses. The elemental maps reveal an almost uniform distribution of all REEs within the particle, with Ce, La, Tb, and Y present in higher concentrations. This finding confirms that the precipitated oxalate consists of a mixed REE oxalate phase, with some calcium sulfate likely crystallized on the particle surface during precipitation.

Similarly, the spectrum of the calcined sample (Supplementary Figure S10-d) exhibits sharper peaks due to the enrichment of elements after thermal decomposition. Elemental mapping of the calcined product further demonstrates increased element concentrations compared to the pre-calcination sample.

4. Process analysis

To evaluate the efficiency of the developed process and determine the total recovery rate, 100 g of spent phosphor powder was processed according to the scheme illustrated in Fig. 5. Initially, the phosphor powder was leached in a 1 M sulfuric acid solution at 80 °C with S/L ratio of 5 % for 1 hour. Following filtration, the majority of Y, Eu, were selectively recovered and precipitated by adding 0.15 M oxalic acid. The solid residue from the leaching step was then mixed with sulfuric acid at an acid-to-powder weight ratio of 2 and subjected to sulfation at 150 °C for 5 h. Afterward, the sulfated sample was leached in water with S/L ratio of 10 % at room temperature for 10 min. The resulting solution was filtered and further treated with 0.3 M oxalic acid to precipitate all REEs.

Mass balance calculations for the entire process revealed an overall

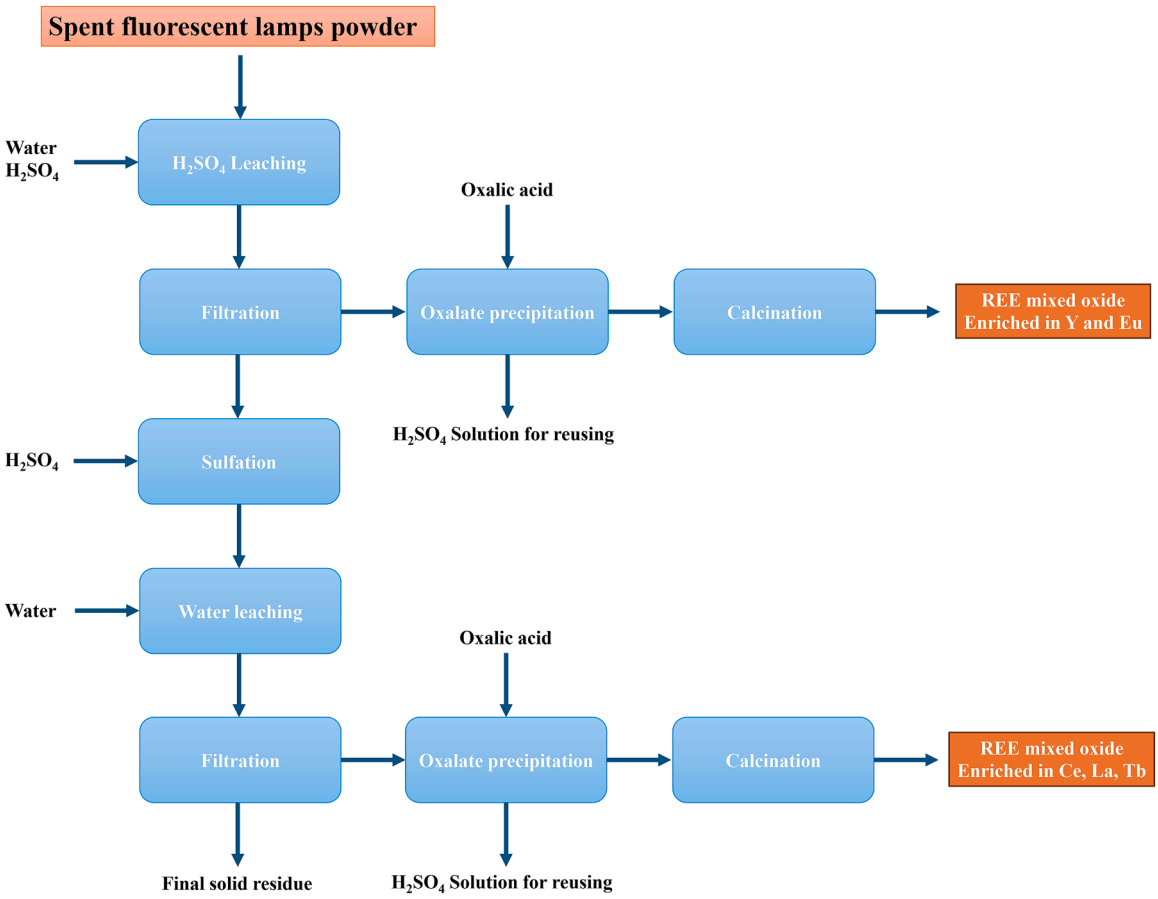

Fig. 5. Process scheme for recovering REEs from spent fluorescent lamps, yielding two separate oxide products: one enriched in Y and Eu, and the other in Ce, La, and Tb.

recovery of 99.98 % Y, 100 % Eu, 99.92 % Ce, 97.22 % La, 97.68 % Tb, and 99.97 % Gd. Supplementary Table S17 presents the distribution of all REEs in both solid and liquid phases at each stage of the process, expressed as a percentage of their total initial content in the spent phosphor powder (100 %). These results demonstrate the high efficiency of the developed method, particularly in the nearly complete recovery of terbium, which is often challenging to extract from spent fluorescent lamp powders. Finally, a preliminary economic analysis was conducted based on approximate reagent costs and mass balance calculations to estimate the cost of treating 1 ton of spent fluorescent lamp powder. In parallel, the potential revenue from the recovery of mixed REE oxides was evaluated, assuming a conservative market value of 50 % of the price of pure REE oxides. The detailed pricing data and calculations are provided in Supplementary Tables S18 and S19.

5. Conclusion

This study presents a comprehensive process for the recovery of rare earth elements from spent fluorescent lamp powder. Sulfuric acid leaching followed by oxalate precipitation enabled the selective recovery of nearly pure yttrium and europium oxalates, with calcium oxalate and sulfate as the primary impurities.

Thermodynamic evaluations established that maintaining the sulfation process at or below 150 °C prevents sulfuric acid and mercury evaporation, an aspect overlooked in previous studies. By conducting sulfation within this safe temperature range, followed by water leaching and oxalate precipitation, almost complete REE recovery was achieved, leaving negligible REE residues in the solid waste. SEM analysis revealed the formation of flower-like REE oxalates and oxides after precipitation, with sulfuric acid regeneration as an additional benefit.

Key findings of this study include:

- Sulfuric acid leaching (1 M H_2SO_4, 80 °C, 1 hour) recovered 98.77 % Y, 95.81 % Eu, 6.78 % Ce, 0.13 % La, 13.17 % Tb, and 67.28 % Gd, along with significant co-dissolution of 47.11 % Al, 37.26 % Ca, 97.24 % Mn, 91.21 % Fe, and 81.79 % B.
- Oxalate precipitation selectively recovered REEs from the leachate, yielding $\alpha > 99$ % pure oxalate mixture, consisting primarily of 93.44 % Y, 4.05 % Eu, 1.12 % Gd, 0.28 % Tb, 0.27 % Ce, and 0.01 % La oxalate hydrates.
- Sulfation at 150 °C for 5 h with an acid-to-powder weight ratio of 2 enabled the recovery of nearly 100 % Eu, Ce, and Gd, 98.79 % Y, 98.01 % La, and 98.15 % Tb from the remaining solid residue.
- The final oxalate precipitate after sulfation-water leaching was >98 % pure, consisting of 43.72 % La, 27.35 % Ce, 14.86 % Tb, 7.31 % Y, 3.97 % Gd, 1.36 % Eu oxalate hydrates, and 1.44 % calcium oxalate and sulfate.

This process demonstrates an effective, environmentally friendly approach for REE recovery, maximizing resource efficiency while minimizing energy consumption and chemical diversity.

Funding

This study was developed within the NEW-RE project (number 21116) which was supported and financed by EIT-RawMaterials.

CRediT authorship contribution statement

Hossein Shalchian: Writing – original draft, Software,

Methodology, Investigation, Formal analysis, Conceptualization. **Pietro Romano:** Writing – review & editing, Writing – original draft, Software, Methodology. **Soroush Rahmati:** Writing – review & editing, Investigation, Formal analysis. **Ionela Birloaga:** Validation, Formal analysis, Data curation. **Valentina Innocenzi:** Visualization, Validation, Data curation. **Francesco Vegliò:** Writing – review & editing, Validation, Supervision, Resources, Project administration, Funding acquisition, Data curation, Conceptualization.

Declaration of competing interest

The authors declare that they have no known competing financial interests or personal relationships that could have appeared to influence the work reported in this paper.

Acknowledgments

The authors thank all the NEW-RE Consortium partners for collaborating in this research activity and Relight Srl dismantling plant for providing the spent fluorescent powder. The authors would like to thank the University of L'Aquila for their precious support.

Supplementary materials

Supplementary material associated with this article can be found, in the online version, at doi:10.1016/j.resconrec.2025.108495.

Data availability

Data will be made available on request.

References

Alcaraz, L., et al., 2022. Extraction of lanthanum oxide from different spent fluid catalytic cracking catalysts by nitric acid leaching and Cyanex 923 solvent extraction methods. Metals 12 (3), 378.
Altaş, Y., Tel, H., 2001. Structural and thermal investigations on cerium oxalate and derived oxide powders for the preparation of (Th, Ce) O2 pellets. J. Nucl. Mater. 298 (3), 316–320.
Bilen, A., Birol, B., Sönmez, M.Ş., 2025. Selective recovery of yttrium oxide and yttrium–europium oxide particles from fluorescent wastes by solvent extraction, precipitation, and calcination. J. Mater. Cycles. Waste Manage 27 (1), 193–208.
Binnemans, K., et al., 2013. Recycling of rare earths: a critical review. J. Clean. Prod. 51, 1–22.
Binnemans, K., Jones, P.T., 2023. The twelve principles of circular hydrometallurgy. J. Sustain. Metall. 9 (1), 1–25.
Chi, R.-A., Xu, Z.-G., 1999. A solution chemistry approach to the study of rare earth element precipitation by oxalic acid. Metall. Mater. Trans. B 30, 189–195.
De Michelis, I., et al., 2011. Treatment of exhaust fluorescent lamps to recover yttrium: experimental and process analyses. Waste Manage. 31 (12), 2559–2568.
Dhapte, A., 2025. Fluorescent Lighting Market Research Report Information By Application (Residential, Commercial, and Industrial), By Installation (New Installation and Retrofit), By Type (Linear Fluorescent Lamps [LFL] and Cold Cathode Fluorescent Lamp [CCFL]), And By Region (North America, Europe, Asia-Pacific, And Rest Of The World) –Industry Forecast Till 2032. JuneAvailable from. https://www.marketresearchfuture.com/reports/fluorescent-lighting-market-8501.
Dhawan, N., Tanvar, H., 2022. A critical review of end-of-life fluorescent lamps recycling for recovery of rare earth values. Sustain. Mater. Technol. 32, e00401.
Han, K.N., 2020. Characteristics of precipitation of rare earth elements with various precipitants. Minerals 10 (2), 178.
Innocenzi, V., et al., 2016. A hydrometallurgical process for the recovery of terbium from fluorescent lamps: experimental design, optimization of acid leaching process and process analysis. J. Env. Manage 184, 552–559.
Innocenzi, V., et al., 2017. Secondary yttrium from spent fluorescent lamps: recovery by leaching and solvent extraction. Int. J. Miner. Process. 168, 87–94.
Innocenzi, V., et al., 2018. Application of solvent extraction operation to recover rare earths from fluorescent lamps. J. Clean. Prod. 172, 2840–2852.
Ippolito, N.M., et al., 2017. Rare earth elements recovery from fluorescent lamps: a new thermal pretreatment to improve the efficiency of the hydrometallurgical process. J. Clean. Prod. 153, 287–298.
Ippolito, N.M., et al., 2021. Effect of mechanical activation on terbium dissolution from waste fluorescent powders. Min. Eng. 167, 106906.
Kim, E., Osseo-Asare, K., 2012. Aqueous stability of thorium and rare earth metals in monazite hydrometallurgy: eh–pH diagrams for the systems Th–, Ce–, La–, Nd–(PO4)–(SO4)–H2O at 25 C. Hydrometallurgy 113, 67–78.
Liascukiene, I., et al., 2021. Morphology-controlled precipitation of cerium oxalate crystals: the effect of water in nanostructured solvents. J. Phys. Chem. C 125 (17), 9428–9440.
Liu, C., et al., 2025. Synergistic recovery of mercury and rare earth elements from waste phosphors by microwave alkali fusion-carbothermal reduction followed by acid leaching. J. Hazard. Mater., 137473
Mesaros, A., et al., 2015. Insights into the europium-doped yttrium oxalate thermal decomposition mechanism. J. Anal. Appl. Pyrolysis. 116, 96–101.
Montgomery, D.C., 2017. Design and Analysis of Experiments. John wiley & sons.
Nawab, A., Yang, X., Honaker, R., 2022. Parametric study and speciation analysis of rare earth precipitation using oxalic acid in a chloride solution system. Min. Eng. 176, 107352.
Önal, M.A.R., Binnemans, K., 2019. Recovery of rare earths from waste cathode ray tube (CRT) phosphor powder by selective sulfation roasting and water leaching. Hydrometallurgy 183, 60–70.
Peng, L., Wang, Y., Chang, C.-T., 2014. Recycling research on spent fluorescent lamps on the basis of extended producer responsibility in China. J. Air Waste Manage Assoc. 64 (11), 1299–1308.
Porob, D.G., et al., 2012. Rare Earth Recovery from Fluorescent Material and Associated Method. Google Patents.
Sadri, F., Nazari, A.M., Ghahreman, A., 2017. A review on the cracking, baking and leaching processes of rare earth element concentrates. J. Rare Earths 35 (8), 739–752.
Shukla, N., Agrawal, S., Dhawan, N., 2021. Microwave acid baking process for recovery of rare-earth concentrate from phosphor of end-of-life fluorescent lamps. J. Clean. Prod. 307, 127235.
Shukla, N., Dhawan, N., 2022. Comparison of processing routes for recovery of rare earth elements from discarded fluorescent lamp phosphors. Min. Eng. 187, 107759.
Silveira, G.T., Chang, S.-Y., 2011. Fluorescent lamp recycling initiatives in the United States and a recycling proposal based on extended producer responsibility and product stewardship concepts. Waste Manage Res. 29 (6), 656–668.
Song, G., et al., 2017. Improvement in rare earth element recovery from waste trichromatic phosphors by mechanical activation. J. Clean. Prod. 151, 361–370.
Tan, Q., Deng, C., Li, J., 2017. Enhanced recovery of rare earth elements from waste phosphors by mechanical activation. J. Clean. Prod. 142, 2187–2191.
Tan, Q., Li, J., 2014. A study of waste fluorescent lamp generation in mainland China. J. Clean. Prod. 81, 227–233.
Tan, Q., Li, J., Zeng, X., 2015. Rare earth elements recovery from waste fluorescent lamps: a review. Crit. Rev. Env. Sci. Technol. 45 (7), 749–776.
Tian, Z., et al., 2025. Alkali fusion deconstruction and rare-earth recovery from hazardous spent fluorescent lamp phosphors: experimental and theoretical calculations. ACS. Sustain. Chem. Eng.
Tunsu, C., Ekberg, C., Retegan, T., 2014. Characterization and leaching of real fluorescent lamp waste for the recovery of rare earth metals and mercury. Hydrometallurgy 144, 91–98.
Van Loy, S., Binnemans, K., Van Gerven, T., 2017. Recycling of rare earths from lamp phosphor waste: enhanced dissolution of LaPO4: ce3+, Tb3+ by mechanical activation. J. Clean. Prod. 156, 226–234.
Vaz, G.V., et al., 2025. A novel method for leaching rare earth element from fluorescent lamp waste via acid fusion. Hydrometallurgy 232, 106420.
Viana, L.N., et al., 2022. Fluorescent lamps: a review on environmental concerns and current recycling perspectives highlighting Hg and rare earth elements. J. Environ. Chem. Eng. 10 (6), 108915.
Wu, Y., et al., 2014. The recycling of rare earths from waste tricolor phosphors in fluorescent lamps: a review of processes and technologies. Resour. Conserv. Recycl. 88, 21–31.